Transverse single spin asymmetries of forward neutrons in $p+p$, $p+\mathrm{Al}$, and $p+\mathrm{Au}$ collisions at $\sqrt{s_{NN}}=200$ GeV as a function of transverse and longitudinal momenta

U. A. Acharya,[20] C. Aidala,[40] Y. Akiba,[53,54,*] M. Alfred,[22] V. Andrieux,[40] N. Apadula,[27] H. Asano,[33,53] B. Azmoun,[7] V. Babintsev,[23] N. S. Bandara,[39] K. N. Barish,[8] S. Bathe,[5,54] A. Bazilevsky,[7] M. Beaumier,[8] R. Belmont,[11,46] A. Berdnikov,[56] Y. Berdnikov,[56] L. Bichon,[64] B. Blankenship,[64] D. S. Blau,[32,43] J. S. Bok,[45] V. Borisov,[56] M. L. Brooks,[35] J. Bryslawskyj,[5,8] V. Bumazhnov,[23] S. Campbell,[12] V. Canoa Roman,[59] R. Cervantes,[59] M. Chiu,[7] C. Y. Chi,[12] I. J. Choi,[24] J. B. Choi,[29,†] Z. Citron,[65] M. Connors,[20,54] R. Corliss,[59] N. Cronin,[59] T. Csörgő,[16,66] M. Csanád,[15] T. W. Danley,[47] M. S. Daugherity,[1] G. David,[7,59] K. DeBlasio,[44] K. Dehmelt,[59] A. Denisov,[23] A. Deshpande,[54,59] E. J. Desmond,[7] A. Dion,[59] D. Dixit,[59] J. H. Do,[67] A. Drees,[59] K. A. Drees,[6] J. M. Durham,[35] A. Durum,[23] H. En'yo,[53] A. Enokizono,[53,55] R. Esha,[59] S. Esumi,[63] B. Fadem,[41] W. Fan,[59] N. Feege,[59] D. E. Fields,[44] M. Finger, Jr.,[9] M. Finger,[9] D. Fitzgerald,[40] S. L. Fokin,[32] J. E. Frantz,[47] A. Franz,[7] A. D. Frawley,[19] Y. Fukuda,[63] P. Gallus,[13] C. Gal,[59] P. Garg,[3,59] H. Ge,[59] M. Giles,[59] F. Giordano,[24] Y. Goto,[53,54] N. Grau,[2] S. V. Greene,[64] M. Grosse Perdekamp,[24] T. Gunji,[10] H. Guragain,[20] T. Hachiya,[42,53,54] J. S. Haggerty,[7] K. I. Hahn,[17] H. Hamagaki,[10] H. F. Hamilton,[1] J. Hanks,[59] S. Y. Han,[17,31] M. Harvey,[61] S. Hasegawa,[28] T. O. S. Haseler,[20] T. K. Hemmick,[59] X. He,[20] J. C. Hill,[27] K. Hill,[11] A. Hodges,[20] R. S. Hollis,[8] K. Homma,[21] B. Hong,[31] T. Hoshino,[21] N. Hotvedt,[27] J. Huang,[7] K. Imai,[28] M. Inaba,[63] A. Iordanova,[8] D. Isenhower,[1] D. Ivanishchev,[51] B. V. Jacak,[59] M. Jezghani,[20] X. Jiang,[35] Z. Ji,[59] B. M. Johnson,[7,20] D. Jouan,[49] D. S. Jumper,[24] J. H. Kang,[67] D. Kapukchyan,[8] S. Karthas,[59] D. Kawall,[39] A. V. Kazantsev,[32] V. Khachatryan,[59] A. Khanzadeev,[51] A. Khatiwada,[35] C. Kim,[8,31] E.-J. Kim,[29] M. Kim,[57] T. Kim,[17] D. Kincses,[15] A. Kingan,[59] E. Kistenev,[7] J. Klatsky,[19] P. Kline,[59] T. Koblesky,[11] D. Kotov,[51,56] L. Kovacs,[15] S. Kudo,[63] K. Kurita,[55] Y. Kwon,[67] J. G. Lajoie,[27] D. Larionova,[56] A. Lebedev,[27] S. Lee,[67] S. H. Lee,[27,40,59] M. J. Leitch,[35] Y. H. Leung,[59] N. A. Lewis,[40] S. H. Lim,[35,52,67] M. X. Liu,[35] X. Li,[35] V.-R. Loggins,[24] D. A. Loomis,[40] K. Lovasz,[14] D. Lynch,[7] S. Lökös,[15] T. Majoros,[14] Y. I. Makdisi,[6] M. Makek,[68] V. I. Manko,[32] E. Mannel,[7] M. McCumber,[35] P. L. McGaughey,[35] D. McGlinchey,[11,35] C. McKinney,[24] M. Mendoza,[8] A. C. Mignerey,[38] A. Milov,[65] D. K. Mishra,[4] J. T. Mitchell,[7] M. Mitrankova,[56] Iu. Mitrankov,[56] G. Mitsuka,[30,54] S. Miyasaka,[53,62] S. Mizuno,[53,63] M. M. Mondal,[59] P. Montuenga,[24] T. Moon,[31,67] D. P. Morrison,[7] B. Mulilo,[31,53] T. Murakami,[33,53] J. Murata,[53,55] K. Nagai,[62] K. Nagashima,[21] T. Nagashima,[55] J. L. Nagle,[11] M. I. Nagy,[15] I. Nakagawa,[53,54] K. Nakano,[53,62] C. Nattrass,[60] S. Nelson,[18] T. Niida,[63] R. Nouicer,[7,54] T. Novák,[16,66] N. Novitzky,[59,63] G. Nukazuka,[53,54] A. S. Nyanin,[32] E. O'Brien,[7] C. A. Ogilvie,[27] J. D. Orjuela Koop,[11] J. D. Osborn,[40,48] A. Oskarsson,[36] G. J. Ottino,[44] K. Ozawa,[30,63] V. Pantuev,[25] V. Papavassiliou,[45] J. S. Park,[57] S. Park,[53,57,59] M. Patel,[27] S. F. Pate,[45] W. Peng,[64] D. V. Perepelitsa,[7,11] G. D. N. Perera,[45] D. Yu. Peressounko,[32] C. E. PerezLara,[59] J. Perry,[27] R. Petti,[7] M. Phipps,[7,24] C. Pinkenburg,[7] R. P. Pisani,[7] M. Potekhin,[7] A. Pun,[47] M. L. Purschke,[7] P. V. Radzevich,[56] N. Ramasubramanian,[59] K. F. Read,[48,60] D. Reynolds,[58] V. Riabov,[43,51] Y. Riabov,[51,56] D. Richford,[5] T. Rinn,[24,27] S. D. Rolnick,[8] M. Rosati,[27] Z. Rowan,[5] J. Runchey,[27] A. S. Safonov,[56] T. Sakaguchi,[7] H. Sako,[28] V. Samsonov,[43,51] M. Sarsour,[20] S. Sato,[28] B. Schaefer,[64] B. K. Schmoll,[60] K. Sedgwick,[8] R. Seidl,[53,54] A. Sen,[27,60] R. Seto,[8] A. Sexton,[38] D. Sharma,[59] I. Shein,[23] T.-A. Shibata,[53,62] K. Shigaki,[21] M. Shimomura,[27,42] T. Shioya,[63] P. Shukla,[4] A. Sickles,[24] C. L. Silva,[35] D. Silvermyr,[36] B. K. Singh,[3] C. P. Singh,[3] V. Singh,[3] M. Slunečka,[9] K. L. Smith,[19] M. Snowball,[35] R. A. Soltz,[34] W. E. Sondheim,[35] S. P. Sorensen,[60] I. V. Sourikova,[7] P. W. Stankus,[48] S. P. Stoll,[7] T. Sugitate,[21] A. Sukhanov,[7] T. Sumita,[53] J. Sun,[59] Z. Sun,[14] J. Sziklai,[66] K. Tanida,[28,54,57] M. J. Tannenbaum,[7] S. Tarafdar,[64,65] A. Taranenko,[43] G. Tarnai,[14] R. Tieulent,[20,37] A. Timilsina,[27] T. Todoroki,[53,54,63] M. Tomášek,[13] C. L. Towell,[1] R. S. Towell,[1] I. Tserruya,[65] Y. Ueda,[21] B. Ujvari,[14] H. W. van Hecke,[35] J. Velkovska,[64] M. Virius,[13] V. Vrba,[13,26] N. Vukman,[68] X. R. Wang,[45,54] Y. S. Watanabe,[10] C. P. Wong,[20,35] C. L. Woody,[7] L. Xue,[20] C. Xu,[45] Q. Xu,[64] S. Yalcin,[59] Y. L. Yamaguchi,[59] H. Yamamoto,[63] A. Yanovich,[23] I. Yoon,[57] J. H. Yoo,[31] I. E. Yushmanov,[32] H. Yu,[45,50] W. A. Zajc,[12] A. Zelenski,[6] S. Zharko,[56] and L. Zou[8]

(PHENIX Collaboration)

[1]*Abilene Christian University, Abilene, Texas 79699, USA*
[2]*Department of Physics, Augustana University, Sioux Falls, South Dakota 57197, USA*
[3]*Department of Physics, Banaras Hindu University, Varanasi 221005, India*
[4]*Bhabha Atomic Research Centre, Bombay 400 085, India*
[5]*Baruch College, City University of New York, New York, New York 10010 USA*
[6]*Collider-Accelerator Department, Brookhaven National Laboratory, Upton, New York 11973-5000, USA*
[7]*Physics Department, Brookhaven National Laboratory, Upton, New York 11973-5000, USA*

[8]*University of California-Riverside, Riverside, California 92521, USA*
[9]*Charles University, Ovocný trh 5, Praha 1, 116 36 Prague, Czech Republic*
[10]*Center for Nuclear Study, Graduate School of Science, University of Tokyo, 7-3-1 Hongo, Bunkyo, Tokyo 113-0033, Japan*
[11]*University of Colorado, Boulder, Colorado 80309, USA*
[12]*Columbia University, New York, New York 10027 and Nevis Laboratories, Irvington, New York 10533, USA*
[13]*Czech Technical University, Zikova 4, 166 36 Prague 6, Czech Republic*
[14]*Debrecen University, H-4010 Debrecen, Egyetem tér 1, Hungary*
[15]*ELTE, Eötvös Loránd University, H-1117 Budapest, Pázmány P. s. 1/A, Hungary*
[16]*Eszterházy Károly University, Károly Róbert Campus, H-3200 Gyöngyös, Mátrai út 36, Hungary*
[17]*Ewha Womans University, Seoul 120-750, Korea*
[18]*Florida A&M University, Tallahassee, Florida 32307, USA*
[19]*Florida State University, Tallahassee, Florida 32306, USA*
[20]*Georgia State University, Atlanta, Georgia 30303, USA*
[21]*Hiroshima University, Kagamiyama, Higashi-Hiroshima 739-8526, Japan*
[22]*Department of Physics and Astronomy, Howard University, Washington, DC 20059, USA*
[23]*IHEP Protvino, State Research Center of Russian Federation, Institute for High Energy Physics, Protvino 142281, Russia*
[24]*University of Illinois at Urbana-Champaign, Urbana, Illinois 61801, USA*
[25]*Institute for Nuclear Research of the Russian Academy of Sciences, prospekt 60-letiya Oktyabrya 7a, Moscow 117312, Russia*
[26]*Institute of Physics, Academy of Sciences of the Czech Republic, Na Slovance 2, 182 21 Prague 8, Czech Republic*
[27]*Iowa State University, Ames, Iowa 50011, USA*
[28]*Advanced Science Research Center, Japan Atomic Energy Agency, 2-4 Shirakata Shirane, Tokai-mura, Naka-gun, Ibaraki-ken 319-1195, Japan*
[29]*Jeonbuk National University, Jeonju 54896, Korea*
[30]*KEK, High Energy Accelerator Research Organization, Tsukuba, Ibaraki 305-0801, Japan*
[31]*Korea University, Seoul 02841, Korea*
[32]*National Research Center "Kurchatov Institute", Moscow 123098 Russia*
[33]*Kyoto University, Kyoto 606-8502, Japan*
[34]*Lawrence Livermore National Laboratory, Livermore, California 94550, USA*
[35]*Los Alamos National Laboratory, Los Alamos, New Mexico 87545, USA*
[36]*Department of Physics, Lund University, Box 118, SE-221 00 Lund, Sweden*
[37]*IPNL, CNRS/IN2P3, Univ Lyon, Universit Lyon 1, F-69622 Villeurbanne, France*
[38]*University of Maryland, College Park, Maryland 20742, USA*
[39]*Department of Physics, University of Massachusetts, Amherst, Massachusetts 01003-9337, USA*
[40]*Department of Physics, University of Michigan, Ann Arbor, Michigan 48109-1040, USA*
[41]*Muhlenberg College, Allentown, Pennsylvania 18104-5586, USA*
[42]*Nara Women's University, Kita-uoya Nishi-machi Nara 630-8506, Japan*
[43]*National Research Nuclear University, MEPhI, Moscow Engineering Physics Institute, Moscow 115409, Russia*
[44]*University of New Mexico, Albuquerque, New Mexico 87131, USA*
[45]*New Mexico State University, Las Cruces, New Mexico 88003, USA*
[46]*Physics and Astronomy Department, University of North Carolina at Greensboro, Greensboro, North Carolina 27412, USA*
[47]*Department of Physics and Astronomy, Ohio University, Athens, Ohio 45701, USA*
[48]*Oak Ridge National Laboratory, Oak Ridge, Tennessee 37831, USA*
[49]*IPN-Orsay, University Paris-Sud, CNRS/IN2P3, Université Paris-Saclay, BP1, F-91406 Orsay, France*
[50]*Peking University, Beijing 100871, People's Republic of China*
[51]*PNPI, Petersburg Nuclear Physics Institute, Gatchina, Leningrad region, 188300, Russia*
[52]*Pusan National University, Pusan 46241, Korea*
[53]*RIKEN Nishina Center for Accelerator-Based Science, Wako, Saitama 351-0198, Japan*
[54]*RIKEN BNL Research Center, Brookhaven National Laboratory, Upton, New York 11973-5000, USA*
[55]*Physics Department, Rikkyo University, 3-34-1 Nishi-Ikebukuro, Toshima, Tokyo 171-8501, Japan*
[56]*Saint Petersburg State Polytechnic University, St. Petersburg 195251, Russia*
[57]*Department of Physics and Astronomy, Seoul National University, Seoul 151-742, Korea*
[58]*Chemistry Department, Stony Brook University, SUNY, Stony Brook, New York 11794-3400, USA*

[59]Department of Physics and Astronomy, Stony Brook University, SUNY, Stony Brook, New York 11794-3800, USA
[60]University of Tennessee, Knoxville, Tennessee 37996, USA
[61]Texas Southern University, Houston, Texas 77004, USA
[62]Department of Physics, Tokyo Institute of Technology, Oh-okayama, Meguro, Tokyo 152-8551, Japan
[63]Tomonaga Center for the History of the Universe, University of Tsukuba, Tsukuba, Ibaraki 305, Japan
[64]Vanderbilt University, Nashville, Tennessee 37235, USA
[65]Weizmann Institute, Rehovot 76100, Israel
[66]Institute for Particle and Nuclear Physics, Wigner Research Centre for Physics, Hungarian Academy of Sciences (Wigner RCP, RMKI) H-1525 Budapest 114, POBox 49, Budapest, Hungary
[67]Yonsei University, IPAP, Seoul 120-749, Korea
[68]Department of Physics, Faculty of Science, University of Zagreb, Bijenička c. 32 HR-10002 Zagreb, Croatia

(Received 18 October 2021; accepted 6 January 2022; published 11 February 2022)

In 2015 the PHENIX collaboration at the Relativistic Heavy Ion Collider recorded $p+p$, $p+\mathrm{Al}$, and $p+\mathrm{Au}$ collision data at center of mass energies of $\sqrt{s_{NN}}=200$ GeV with the proton beam(s) transversely polarized. At very forward rapidities $\eta>6.8$ relative to the polarized proton beam, neutrons were detected either inclusively or in (anti)correlation with detector activity related to hard collisions. The resulting single spin asymmetries, that were previously reported, have now been extracted as a function of the transverse momentum of the neutron as well as its longitudinal momentum fraction x_F. The explicit kinematic dependence, combined with the correlation information allows for a closer look at the interplay of different mechanisms suggested to describe these asymmetries, such as hadronic interactions or electromagnetic interactions in ultraperipheral collisions, UPC. Events that are correlated with a hard collision indeed display a mostly negative asymmetry that increases in magnitude as a function of transverse momentum with only little dependence on x_F. In contrast, events that are not likely to have emerged from a hard collision display positive asymmetries for the nuclear collisions with a kinematic dependence that resembles that of a UPC based model. Because the UPC interaction depends strongly on the charge of the nucleus, those effects are very small for $p+p$ collisions, moderate for $p+\mathrm{Al}$ collisions, and large for $p+\mathrm{Au}$ collisions.

DOI: 10.1103/PhysRevD.105.032004

I. INTRODUCTION

Very forward particle production in hadronic collisions has gained interest in the past decades due to its connection to other fields of science such as ultrahigh-energy cosmic air showers. Such processes can be studied in controlled collisions to better calibrate their behavior. Given that at very forward regions the momentum transfer scales are often too small to describe the scattering process by perturbative quantum chromodynamics, nonperturbative descriptions of the strong interaction are needed to describe these processes. The simplest description is given by the exchange of a meson between the two beam hadrons. In Regge theory, very forward (but not necessarily very hard) processes were described by the exchange of the lightest hadrons between the colliding nucleons or nuclei, most dominantly by pions. Such calculations describe the measured forward neutron cross sections [1] reasonably well [2].

The well-known forward neutron single spin asymmetries that were discovered in $p+p$ collisions [3–5], though, could not be directly explained by one-pion exchange, OPE, alone. However, by adding the interference between pions and a_1 resonances such single hadron exchange models could also create asymmetries [6]. This picture seemed to describe the measured forward neutron asymmetries in $p+p$ collisions reasonably well. The discovery of very different asymmetries in proton-nucleus collisions [7] came initially as a big surprise because the sign and the magnitude of the asymmetries were quite different than the expectations. Very rapidly after these discoveries the impact of other contributions, most importantly electromagnetic interactions in ultraperipheral

*PHENIX Spokesperson: akiba@rcf.rhic.bnl.gov
†Deceased

collisions (UPC) was realized [8]. UPC describe the process where one nucleon or nucleus emits photons that then interact with the particle of the other beam. As it is an electromagnetic interaction, it can still take place when the impact parameters between the colliding nucleons or nuclei become too large for the strong interaction to contribute.

The interplay of the UPC interaction and hadronic interactions qualitatively describes the measured neutron asymmetries in proton-proton ($p+p$), proton-aluminum ($p+\mathrm{Al}$) and proton-gold ($p+\mathrm{Au}$) collisions, taking into account that the electromagnetic UPC interaction strongly depends on the charge of the colliding nucleus. The contributions based on pion-a_1 interference contain a nearly linearly rising transverse momentum p_T dependence (relative to the beam direction) while the dependence on the longitudinal momentum fraction x_F (normalized by the beam momentum) is very weak. In contrast, the UPC related asymmetries depend strongly on the nucleon resonances that can be produced out of the transversely polarized proton and their subsequent decay kinematics. As such, the asymmetries are expected to change as a function of the neutron p_T and x_F. For this purpose this paper extracts the single spin asymmetries of forward neutrons as a function of p_T and x_F in $p+p$, $p+\mathrm{Al}$ and $p+\mathrm{Au}$ collisions. In the previous paper [9], only the transverse momentum dependence of the single spin asymmetries in $p+p$ collisions was extracted. In addition, in each collision system the neutron single spin asymmetries are extracted for inclusive neutrons, as well as in (anti) coincidence with hard-collision sensitive detector activity. These correlated results provide additional insights into the hadronic and UPC interactions as they either enhance or suppress either one of the contributions.

This paper is organized as follows. Initially the various data sets, necessary Monte Carlo simulations and the PHENIX detector systems relevant for this analysis are presented in Sec. II. Then the event and neutron selection are explained in Sec. III and the asymmetry extraction and unfolding of the raw asymmetries are presented in Sec. IV. The results are discussed in Sec. V before the paper is summarized.

II. DATASETS AND MONTE CARLO SIMULATIONS

In 2015 the PHENIX experiment has taken data colliding transversely polarized proton beams with also transversely polarized proton beams, as well as Al and Au beams. The PHENIX detector is described in detail in Ref. [10]. Here only the detectors relevant for the following results are presented. Forward neutrons are detected with the zero degree calorimeter (ZDC) which comprise three modules of Cu-W alloy absorbers that are layered with optical fibers. Each module corresponds to 1.7 nuclear interaction lengths or 51 radiation lengths and has a projected transverse size of 10 cm by 10 cm with respect to the beam direction. Each of these layers is tilted 45 degrees upward to optimize the Čerenkov light collection. The ZDCs are located approximately 18 m up and downstream of the PHENIX interaction point but for the presented analysis only the results of the ZDC at the proton-going beam direction are reported. In $p+p$ collisions also the same ZDC as in $p+\mathrm{A}$ collisions has been analyzed, calculating the asymmetries relative to the outgoing proton beam's spin orientation only. Due to the different rigidities of protons and nuclei, the beam direction of the proton beam is tilted in proton-nucleus collisions and the ZDCs have been moved to still be located at the nominal proton-beam center position. The ZDCs cover pseudorapidities of $\eta > 6.8$ and have an energy resolution of about 20% for 100 GeV neutrons. The neutron hit positions are measured at the approximate maximum of the hadronic shower development with scintillator strip detectors between the first and second absorber modules. The strips of this shower-max detector (SMD) have a projected width of 15 mm horizontally and vertically. The hit positions in each direction are evaluated by obtaining the deposited energy weighted average of all strip positions. The SMD position resolutions are $\approx$1 cm in each direction. In addition, the SMDs are used in PHENIX for local polarimetry to confirm the beam spin orientation is rotated in the desired direction by making use of the nonzero neutron asymmetries. In the proton-nucleus collisions, hodoscopes upstream of the ZDC were used to reject charged particles that potentially spray into the ZDCs from the magnet that merges and separates the two beams. These detectors were not installed in the $p+p$ collisions period in 2015 and charged backgrounds were subtracted using their background contributions from the 2008 running period where these charge-veto detectors were available.

The correlation analysis used the beam-beam counters (BBCs), which are located at 144 cm up and downstream of the nominal interaction point and cover pseudorapidities of $3.1 < |\eta| < 3.9$. The BBCs comprise of 64 quartz crystals, each being connected to photomultiplier tubes, and are sensitive to predominantly hard interactions. They provide the beam interaction vertex and timing information for most events. Both ZDCs and BBCs are used for event triggering and the BBCs are generally the basis for more sophisticated triggers that include other detector subsystems.

Various Monte Carlo (MC) generators were prepared to evaluate the uncertainties in the production of very forward neutrons. All of them were then piped through full GEANT3 [11] simulations that include the ZDCs, the BBCs, the beam pipe, as well as the magnetic field of the dipole magnet that joins and separates the two beams. The three MC generators DPMJET [12], PYTHIA6.2 [13] and PYTHIA8.2 [14] generally describe a large variety of measurements reasonably well, but usually are more successful with hard interactions. As mentioned in the Introduction, the very forward neutron production is very successfully described

by one-pion exchange. Using an extracted two-dimensional very forward neutron distribution, neutrons are randomly created and the momentum and energy balance to the incoming proton is collided as a pion with the other beam using PYTHIA8.2 again. This allows one to create not only the very forward neutrons, but also the activity in the BBCs for the correlation studies. Last, the UPC interaction was simulated by creating the photon flux from the nuclear beam with the STARLIGHT [15] generator and colliding it with the proton beam.

III. EVENT AND PARTICLE SELECTION CRITERIA

For the inclusive and BBC-vetoed neutron measurements, events were selected via the ZDC triggers that require activity in at least one of the ZDCs and a deposited energy above 15 GeV. For the BBC-tagged neutron measurements events have been triggered via the BBCs, requiring at least one tube to fire per side. Neutrons are detected by the ZDCs if the reconstructed energy from all three modules is between 40 and 120 GeV. To remove electromagnetic particles at least 3% of the total energy has to be accumulated in the second module. At least one hit in each of the horizontal and vertical SMD strips is required to determine the hit position. The radial hit position of the neutron then has to be between 0.5 and 4 cm to avoid acceptance effects as well as to avoid ambiguities in the azimuthal angles. Using the hit radius r and the reconstructed energy E, the transverse momentum p_T of the neutron can be extracted:

$$p_T = \frac{r}{z_{\mathrm{ZDC}}} E, \tag{1}$$

where z_{ZDC} is the z position of the ZDC relative to the beam interaction point. The longitudinal momentum fraction is then calculated as:

$$x_F = \frac{\sqrt{E^2 - p_T^2}}{\sqrt{s_{NN}}/2}, \tag{2}$$

in which the longitudinal momentum is normalized by the beam energy. For the correlated measurements the BBC-tagged events require activity in at least one tube per side, while BBC-vetoed events were selected when neither side has any activity.

IV. ASYMMETRY EXTRACTION AND UNFOLDING

The asymmetries are obtained by selecting neutron candidates in 4 transverse momentum bins from $[0.01, 0.06, 0.11, 0.16, 0.21]$ GeV/c plus one bin below ($[0.00, 0.01]$ GeV/c) and above ($[0.21, 0.40]$ GeV/c) for the unfolding procedure. In x_F also 4 bins from $[0.4, 0.55, 0.7, 0.86, 1.0]$ GeV/c are considered with again two boundary bins below ($[0.0, 0.4]$ GeV/c) and above ($[1.0, 1.2]$ GeV/c) that only can be filled either by the true MC or the smeared data, respectively. The azimuthal angles are binned in 6 equidistant bins that cover the full azimuth where the angle is calculated with respect to the spin-up direction of the polarized proton beam. The asymmetries are then evaluated in each of these bins according to

$$A_N(\phi) = \frac{1}{P} \frac{N^{\uparrow}(\phi) - \mathcal{R} N^{\downarrow}(\phi)}{N^{\uparrow}(\phi) + \mathcal{R} N^{\downarrow}(\phi)}, \tag{3}$$

where $N^{\uparrow}$, $N^{\downarrow}$ are the neutron yields with the polarized proton beam spin orientation up or down, respectively. $\mathcal{R}$ represents the ratio of accumulated luminosities in these spin orientations that the PHENIX experiment sampled and is close to unity. P is the average beam polarization which is 51.5%, 59.4%, and 59.1% for $p+p$, $p+\mathrm{Al}$, and $p+\mathrm{Au}$ collisions, respectively. In the case of $p+p$ collisions the spin orientation of the other beam was averaged over. The asymmetries are then fit with a sine modulation where for systematic studies phase and absolute normalization were left to vary as well.

The raw asymmetries were confirmed by using the so-called square-root method:

$$A_N = \frac{1}{P} \frac{\sqrt{N^{\uparrow}(\phi) N^{\downarrow}(\phi+\pi)} - \sqrt{N^{\downarrow}(\phi) N^{\uparrow}(\phi+\pi)}}{\sqrt{N^{\uparrow}(\phi) N^{\downarrow}(\phi+\pi)} + \sqrt{N^{\downarrow}(\phi) N^{\uparrow}(\phi+\pi)}}, \tag{4}$$

where the geometric mean of left/right yields in the detector cancels out differences in detector acceptance as well as differences in luminosities between the two spin orientations. Both results were found to be consistent with each other and no systematic uncertainty was assigned to it.

Due to the energy and position smearing, the kinematic values need to be unfolded. Unlike the previous publication [9], for the inclusive neutron asymmetries in $p+p$ collisions, the unfolding was performed using the Bayes unfold method [16] as implemented in one (of various) methods in the RooUnfold [17] package of Root [18]. The advantage of using this unfolding package is that three-dimensional unfolding is directly available which is needed in this analysis. Also, the fact that the spin dependent yields (which implicitly contain the asymmetries) will not *a priori* be very similar to the (unpolarized) MC truth distributions is iteratively addressed in the Bayes unfolding. Therefore, one does not need to artificially create spin dependent true MC yields by reweighting the MC according to various asymmetry assumptions. As a consequence, the large uncertainties related to reasonable asymmetry parametrizations used in the reweighting for the TSVDunfolding [19] of the previous publication [9] are not needed here, and the result is substantially reduced overall uncertainties. In this paper the azimuthal angle ϕ, the transverse momentum p_T and the longitudinal momentum fraction

x_F are simultaneously unfolded on the spin-dependent yield level. From the unfolded spin dependent yields the resulting single spin asymmetries were again calculated as described above.

Following the Bayes-unfolding documentation on optimizing the unfolding, the number of iterations was varied around the value of four iterations by one. The variation in the resulting asymmetries was assigned as a systematic uncertainty due to the unfolding procedure. Because the unfolding converges very rapidly, this uncertainty is nearly negligible in the total systematic uncertainties. Similar to the previous publication [9], the variation of the unfolded asymmetries when using the different MC generators was also assigned as a systematic uncertainty. However, given that this unfolding method is much less sensitive to the MC input distributions these uncertainties are rather minor for most asymmetries. Only the impact of statistics at the edges of the dedicated MCs are visible. For the correlated asymmetries the unfolding was performed either on the full MC samples or applying the correlation selection also for the MC samples. This variation was also included as systematic uncertainty and reached up to a few percent.

Further sources of uncertainties were charged particle backgrounds in the $p + p$ collisions where the uncertainties on the relative background fractions were assigned to the spin-dependent yields. The variations in yields were also unfolded to result in uncertainties on the asymmetries. Next, the projected beam center position relative to the center of the ZDCs was varied by one cm in the horizontal and vertical directions. This variation was motivated by the position resolution of the SMD and potential changes in the beam conditions. The corresponding yields were then recalculated, unfolded and the variation of the resulting asymmetries' variation was again assigned as a systematic uncertainty. In many kinematic bins, this is the dominating uncertainty of this measurement. Lastly, as the asymmetries were normalized by the beam polarizations, the uncertainty on these values also enters the asymmetries. For the 2015 running period it was evaluated by the Relativistic-Heavy-Ion-Collider polarimetry group to be 3.4% [20].

The central values in p_T and x_F of the asymmetries do not contain any remaining uncertainties as the smearing was explicitly unfolded. Any differences potentially originating from the different MC generators are already absorbed in the corresponding systematic uncertainties

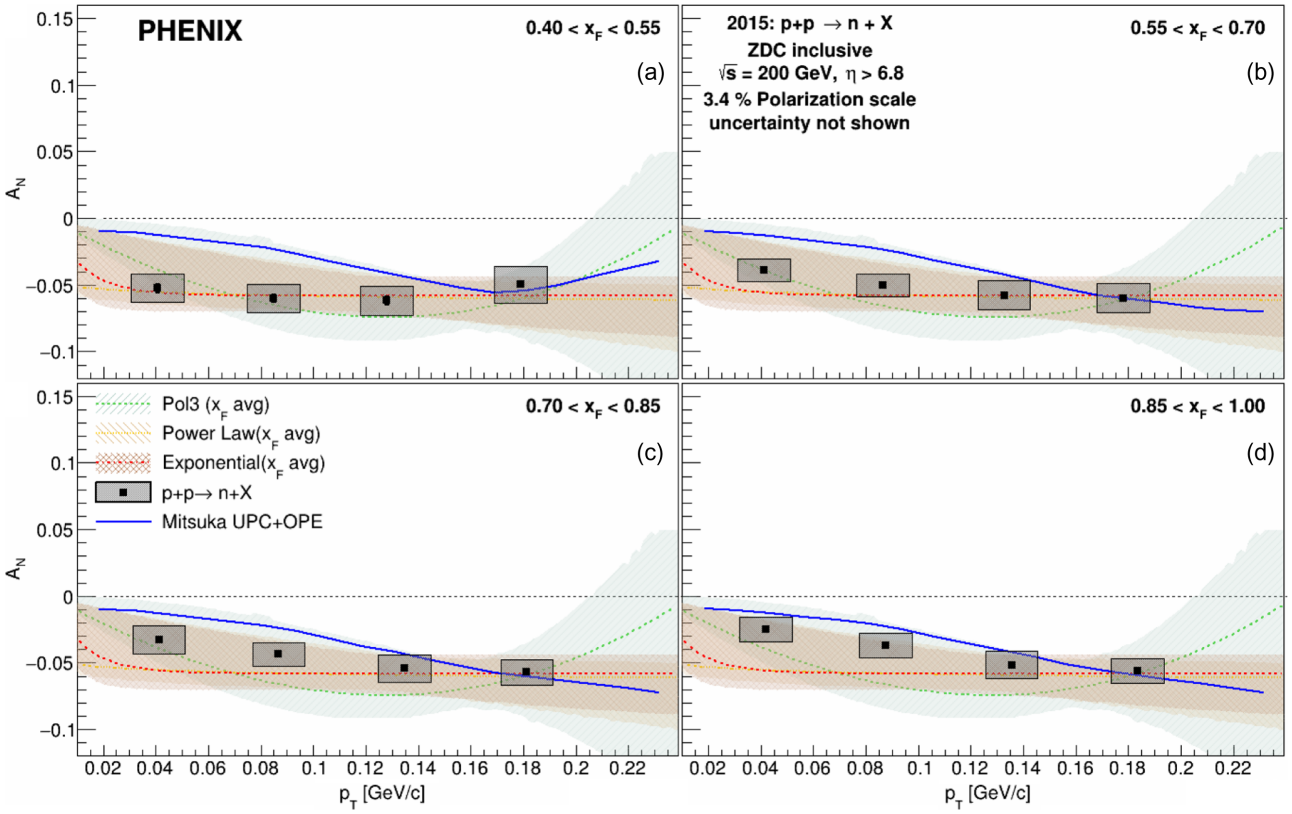

FIG. 1. Single spin asymmetries A_N for very forward inclusive neutrons in $p + p$ collisions as a function of transverse momentum p_T, in bins of x_F. The error boxes represent the systematic uncertainties of the asymmetries while the solid [blue] lines represent the theory calculations. The size of the uncertainty boxes does not reflect the bin boundaries and is chosen for visualization purposes. The three [colored] lines and shaded regions display the asymmetries from the reweighted MC that best describe the measured asymmetries integrated over all x_F bins.

described above. The central values in transverse momentum agree to the third digit between MC generators, while x_F for the UPC generator differs up to 20% from the other generators.

Similar to the previous publication [9], the OPE MC was artificially reweighted to create single spin asymmetries. These weights were based on the following three functional forms: a third-order polynomial, a power-law behavior, and a negative exponential in the true neutron transverse momentum. These curves are not used in the unfolding, but are kept for comparison with the unfolded results. Again the curves that best reproduce the reconstructed asymmetries are expressed by lines for each functional form and the regions with a χ^2 between reconstructed and smeared results below 40 are shaded as well. Because this reweighting exercise was performed over the x_F integrated data and MC, these curves also serve to compare the x_F dependent variations.

V. RESULTS

Before discussing the final results, the theory calculations that are used for comparison of the asymmetries need to be discussed. The calculations comprise the aforementioned hadronic interactions of Ref. [6] and the UPC based calculations of Ref. [8]. In Ref. [21] both contributions have been combined, taking into account the mass number dependence of the hadronic interaction from Ref. [22] as described in Ref. [23]. In these calculations, the unpolarized neutron cross sections for OPE interactions are estimated to be 2.1 mb for $p+p$ collisions, 8.3 mb for $p+\mathrm{Al}$ collisions and 9.4 mb for $p+\mathrm{Au}$ collisions for neutron rapidities above 6.9 and $x_F > 0.4$. In contrast, the estimated UPC-based contributions are below 0.1 mb for $p+p$ collisions, 0.7 mb for $p+\mathrm{Al}$ collisions and 19.6 mb for $p+\mathrm{Au}$ collisions [8].

The calculated asymmetries for hadronic interactions are generally negative and increasing in magnitude with transverse momentum and essentially display no x_F dependence. The UPC-based predictions display a more subtle structure based on the resonances that can be produced initially and their corresponding decay kinematics. At lower transverse momenta the Δ resonance dominantly contributes and creates positive asymmetries overall that are increasing with transverse momentum. At higher transverse momenta other resonances and their three-body

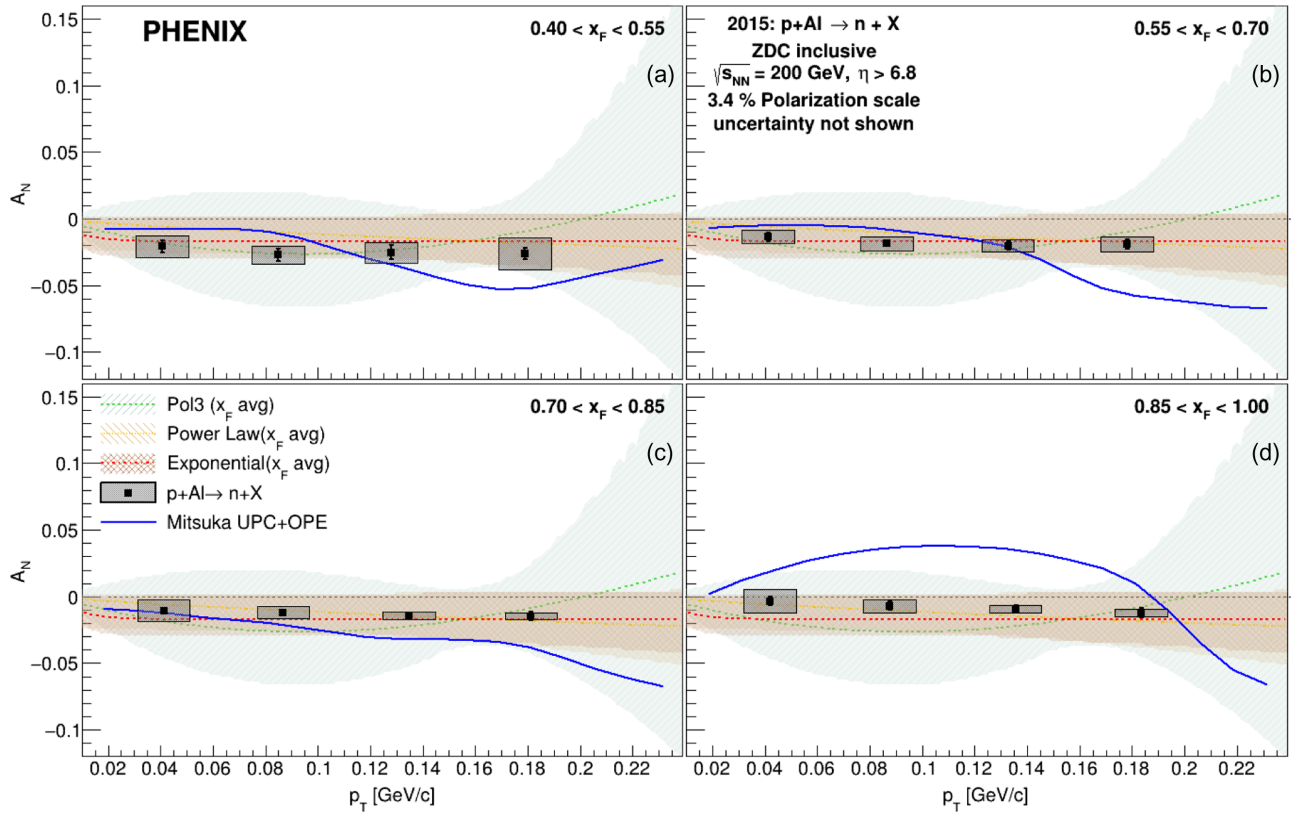

FIG. 2. Single spin asymmetries A_N for very forward inclusive neutrons in $p+\mathrm{Al}$ collisions as a function of transverse momentum p_T, in bins of x_F. The error boxes represent the systematic uncertainties of the asymmetries while the solid [blue] lines represent the theory calculations. The size of the uncertainty boxes does not reflect the bin boundaries and is chosen for visualization purposes. The three [colored] lines and shaded regions display the asymmetries from the reweighted MC that best describe the measured asymmetries integrated over all x_F bins.

decays may also contribute, but are not included in the polarized theory calculation. Therefore the theory calculations predict lower asymmetries. Also the x_F dependence of the UPC-based asymmetry calculations appears to be varying to some extent.

The current MAID-based asymmetry projections [24] are limited to invariant masses below 2 GeV$/c^2$ and resonance decays into a single pion in addition to the neutron while other resonances and decays likely also contribute (as seen, for example, in the unpolarized STARLIGHT-based simulations). As a consequence the sharp asymmetry behavior in the studied phase-space may be smoother and in particular may not exhibit such a sharp drop of the asymmetries at slightly higher transverse momenta. In the case of the correlated asymmetries, in addition to these cross section and asymmetry calculations also their relative reconstruction efficiencies need to be taken into account. These efficiencies are taken from the full GEANT3 simulations. Within the OPE simulations, the efficiencies to fulfill the BBC tagging requirement are predominantly flat in neutron transverse momentum and drop from nearly 65% at small x_F to close to zero when x_F approaches unity. Conversely, the BBC-veto efficiencies range from 15%–20% at low x_F to about 35% close to unity. Overall, within this generator 35% and 17% of all detected neutron events get selected by BBC-tag and BBC-veto, respectively. Note that the remainder of events can be found having only one side of the BBCs showing activity. The other hadronic simulations also show a similar behavior with the actual numbers varying by several percent. In contrast, the UPC simulations have almost no activity in the BBCs with the BBC-veto efficiencies ranging around 85%, and the BBC-tagging efficiencies are at or below 5% throughout the kinematic space covered in these measurements. Overall, 82% of detected neutron events from this generator get selected in the BBC-vetoed case while the BBC-tagged fraction is below one percent. However, other backgrounds such as beam-gas interactions may still create random BBC activity.

Figure 1 shows the results for inclusive $p + p$ collisions as a function of transverse momentum and in bins of x_F. The asymmetries are negative in the whole kinematic region accessed by these measurements. They display a slightly increasing magnitude with increasing transverse momentum except for the lowest x_F bin where the magnitude appears to decrease again. In $p + p$ collisions the interactions are dominated by the hadronic processes

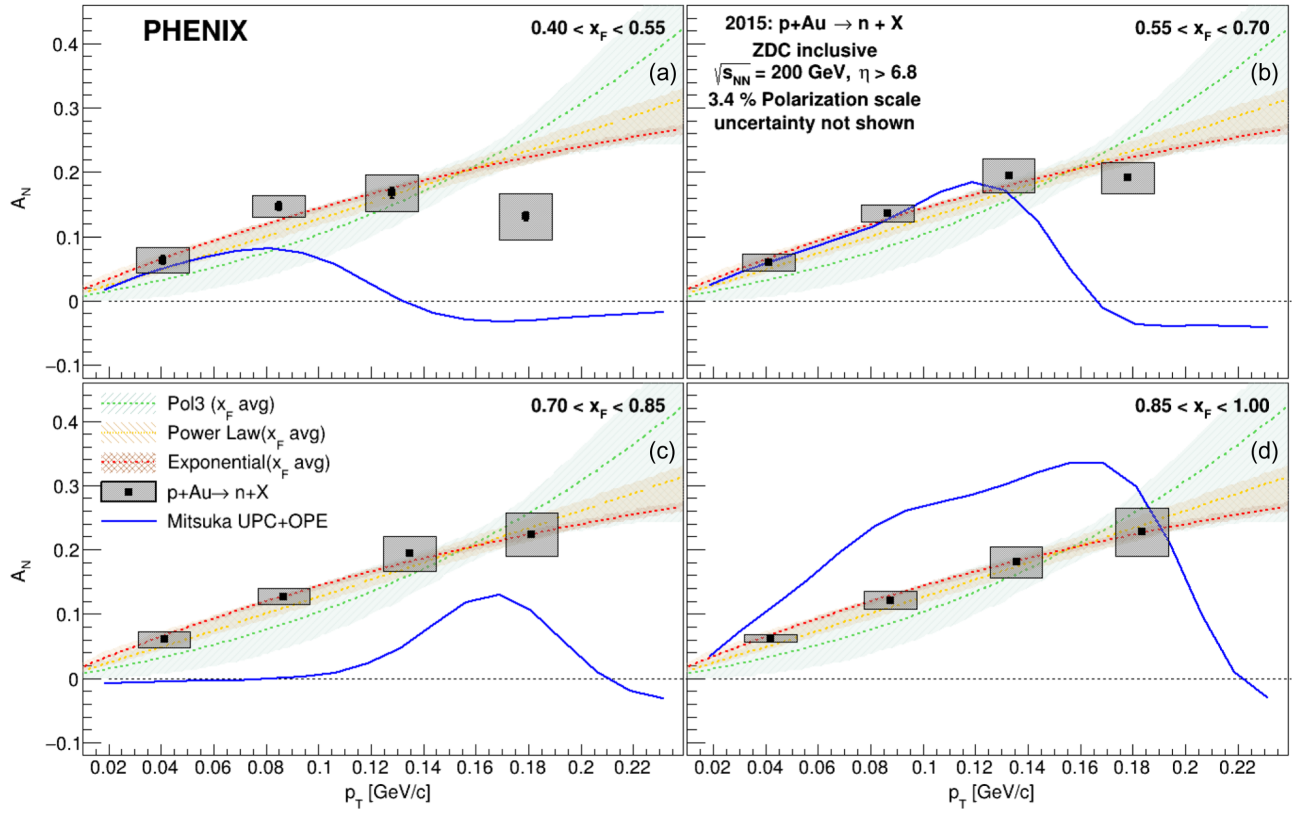

FIG. 3. Single spin asymmetries A_N for very forward inclusive neutrons in $p + \mathrm{Au}$ collisions as a function of transverse momentum p_T, in bins of x_F. The error boxes represent the systematic uncertainties of the asymmetries while the solid [blue] lines represent the theory calculations. The size of the uncertainty boxes does not reflect the bin boundaries and is chosen for visualization purposes. The three [colored] lines and shaded regions display the asymmetries from the reweighted MC that best describe the measured asymmetries integrated over all x_F bins.

and hence the theory calculations are mostly negative and increasing in magnitude. Apart from the lowest x_F bin, they describe the measured asymmetries well.

When studying the inclusive neutron asymmetries in $p+\mathrm{Al}$ collisions, the contribution from UPC events which follows the charge squared of the heavy nucleus will play a larger, but not yet dominating role in the interaction. As a consequence the mostly positive asymmetries from the UPC interaction and the mostly negative asymmetries from the hadron interaction cancel out to a large part as can be seen in Fig. 2. Indeed, the asymmetries are only slightly negative and are often consistent with zero. The theory calculations are again describing the data mostly well. At high x_F some discrepancy is visible where a larger impact of the UPC events is predicted.

In the case of the $p+\mathrm{Au}$ collisions UPC events dominate the interaction and thus the asymmetries become positive as shown in Fig. 3. The asymmetries are rising with increasing transverse momentum in all x_F bins in a similar manner and reach more than 20%. At lower x_F there is an indication of the asymmetries saturating or even falling again which is qualitatively also seen in the theory predictions. The theory calculations show a substantial drop in the asymmetries at higher p_T which is caused by moving away from the Δ resonance where the asymmetries decrease in the UPC calculations. The inclusion of other resonances in these calculations could contribute also in the asymmetries, as they have at least been shown to contribute in unpolarized calculations and the UPC MC generator. This likely also explains the smaller predicted asymmetries at lower p_T in the $0.7 < x_F < 0.85$ region where Δ decays also cannot contribute. Again apart from these highest p_T points, one can see that the x_F dependence is mostly weak which can be seen when comparing with the x_F averaged MC reweighting curves.

In the case of the correlated asymmetries the relative weights of the hadronic and ultraperipheral interactions needed to be added to the theory calculations based on the OPE and UPC MC simulations mentioned above. Generally, a large fraction of hadronic events also fire the BBCs as there is activity in a wide range of rapidities in addition to the very forward region where the neutrons are detected. In contrast UPC interactions, where photons at relatively small scales only excite the proton to a Δ resonance or other nucleon states, very little activity other than from the decay products of these states is expected.

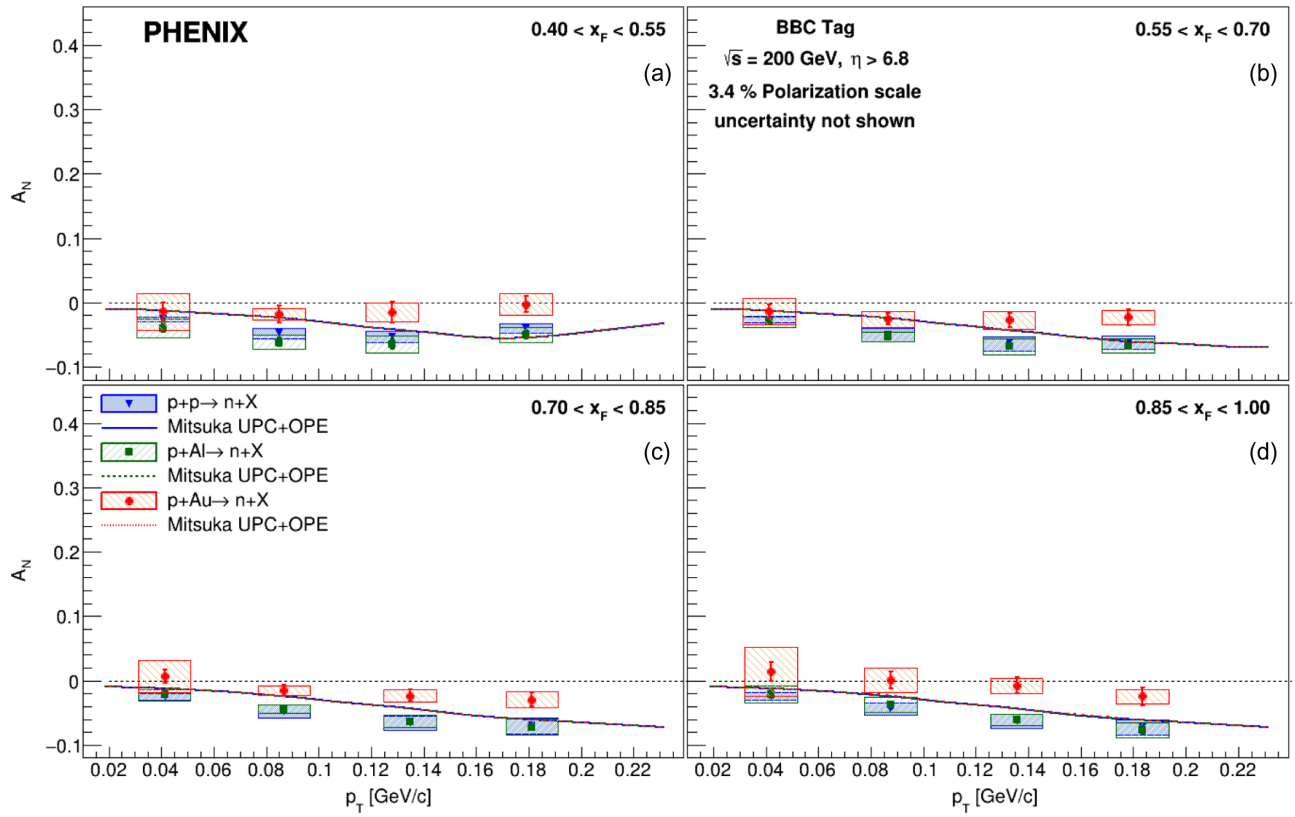

FIG. 4. Single spin asymmetries A_N for very forward neutrons in BBC tagged events in $p+p$ ([blue] triangles and boxes), $p+\mathrm{Al}$ ([green] squares and boxes) and $p+\mathrm{Au}$ ([red] circles and boxes) collisions as a function of transverse momentum p_T, in bins of x_F. The error boxes represent the systematic uncertainties of the asymmetries. The size of the uncertainty boxes does not reflect the bin boundaries and is chosen for visualization purposes. The three [colored] lines represent the theory expectations for $p+p$ ([blue] lines), $p+\mathrm{Al}$ ([green] dashed lines) and $p+\mathrm{Au}$ ([red] dotted lines) as discussed in the text.

Therefore, the overwhelming majority of UPC events do not show any activity in the BBCs. Consequently, the BBC-tagged events are dominated by hadronic interactions and the BBC-vetoed events have a larger UPC contribution depending on the relative contributions of the colliding systems.

Figure 4 displays the BBC-tagged asymmetries as a function of transverse momentum in bins of x_F for $p+p$, $p+\mathrm{Al}$, and $p+\mathrm{Au}$ collisions, respectively. The $p+p$ and the $p+\mathrm{Al}$ asymmetries are indeed negative and show a very similar behavior. The asymmetries are increasing in magnitude more than the inclusive neutron asymmetries and reach magnitudes close to 10%. A nearly linear behavior as predicted by [6] appears to describe these asymmetries rather well as can be seen also in the combined theory calculations that match the data very well. In the lowest x_F bin there is an indication that at higher p_T the asymmetries become smaller again which actually is well described by the combined theory calculations and thus indicates some residual contribution from the UPC interaction. In $p+\mathrm{Au}$ collisions the asymmetries are generally smaller and only are slightly negative at intermediate x_F. This indicates that some UPC events do remain in $p+\mathrm{Au}$ collisions and dilute the predominantly hadronic asymmetries.

In the case of the BBC-vetoed asymmetries the contributions from UPC interactions are enhanced while those from hadronic interactions are reduced but not eliminated. In $p+p$ collisions these two contributions mostly cancel each other out as can be seen in Fig. 5 where the asymmetries are close to zero in most kinematic regions. A hint of a negative asymmetry at lower transverse momenta is still visible but the asymmetries become smaller as the transverse momentum increases. In $p+\mathrm{Al}$ collisions, the larger UPC contribution now switches the sign of the asymmetries to become positive and rising in transverse momentum, reaching up to 10% at the higher transverse momenta. The p_T dependence is again mostly similar for all x_F bins, but at lower x_F the asymmetry in the highest transverse momentum appears to be dropping similar to the inclusive $p+\mathrm{Au}$ collision case. The theory calculations are again qualitatively comparable with the data, including this drop at higher transverse momenta.

In the BBC-vetoed neutron asymmetries of $p+\mathrm{Au}$ collisions the UPC contributions are even further dominant and the resulting asymmetries are even less diluted by the hadronic interactions. This can be seen by the asymmetries now even exceeding 30%. Given the impact of the

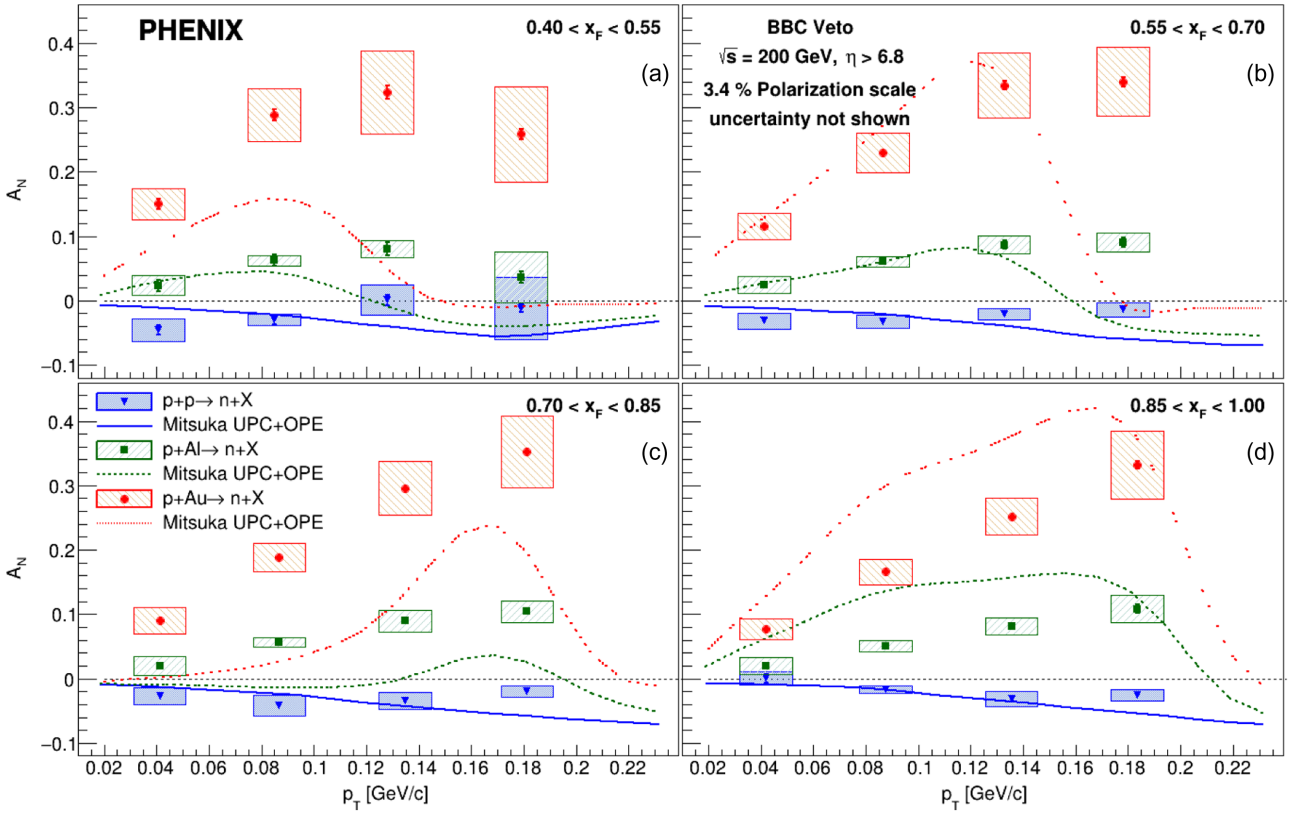

FIG. 5. Single spin asymmetries A_N for very forward neutrons in BBC-vetoed events in $p+p$ ([blue] triangles and boxes), $p+\mathrm{Al}$ ([green] squares and boxes) and $p+\mathrm{Au}$ ([red] circles and boxes) collisions as a function of transverse momentum p_T, in bins of x_F. The error boxes represent the systematic uncertainties of the asymmetries. The size of the uncertainty boxes does not reflect the bin boundaries and is chosen for visualization purposes. The three [colored] lines represent the theory expectations for $p+p$ ([blue] lines), $p+\mathrm{Al}$ ([green] dashed lines) and $p+\mathrm{Au}$ ([red] dotted lines) as discussed in the text.

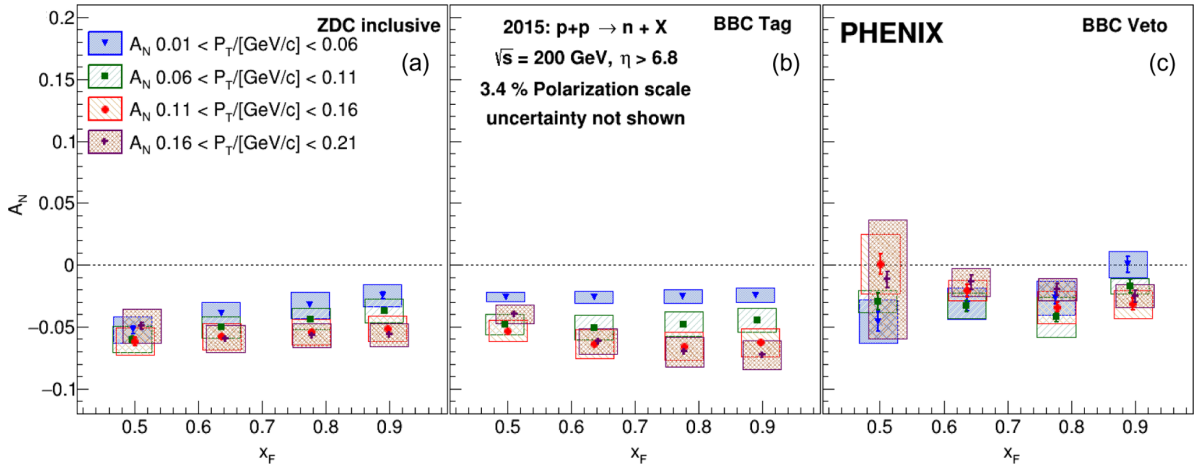

FIG. 6. Single spin asymmetries A_N for very forward neutrons in $p+p$ collisions as a function of x_F, in bins of transverse momentum p_T ([blue] triangles, [green] squares, [red] circles, and [purple] crosses in ascending order). The error boxes represent the systematic uncertainties of the asymmetries. The size of the uncertainty boxes does not reflect the bin boundaries and is chosen for visualization purposes. The three panels display (a) inclusive neutron asymmetries, (b) BBC-tagged neutron asymmetries, and (c) BBC-vetoed neutron asymmetries.

produced nucleon resonances on the decay kinematics, here the largest dependence on x_F can be seen with slightly higher asymmetries at low x_F than in higher bins. The drop of the asymmetries at high p_T at lower x_F noted already in the inclusive $p+\mathrm{Au}$ and the BBC-vetoed $p+\mathrm{Al}$ asymmetries is also visible here.

To look more closely at the x_F dependence, Figs. 6–8 display the same asymmetries as a function of x_F in bins of transverse momentum. In the $p+p$ collisions, within uncertainties, very little dependence on the longitudinal momentum fraction can be seen overall. The only trends can be seen at low transverse momenta for either inclusive or BBC-vetoed neutron events where the magnitude of the asymmetries becomes smaller with increasing x_F. For the BBC-tagged $p+p$ asymmetries, the magnitude for the lowest x_F bin is smaller at higher transverse momenta.

For neutrons in $p+\mathrm{Al}$ collisions, the inclusive neutron asymmetries appear to be getting smaller in magnitude as a function x_F for all transverse momentum bins. This could be an indication that the relative contribution of UPC events becomes stronger with x_F. A similar behavior is also visible for BBC-tagged neutrons, at least for smaller transverse momenta while it is mostly flat in x_F at higher transverse momenta.

In $p+\mathrm{Au}$ collisions, the neutron asymmetries show again generally a weak dependence on x_F. Only in the

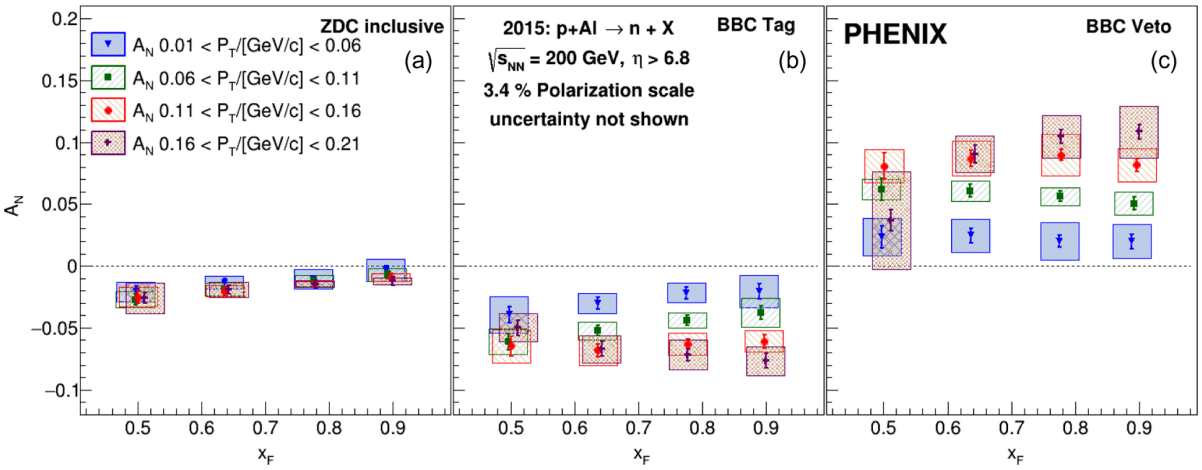

FIG. 7. Single spin asymmetries A_N for very forward neutrons in $p+\mathrm{Al}$ collisions as a function of x_F, in bins of transverse momentum p_T ([blue] triangles, [green] squares, [red] circles, and [purple] crosses in ascending order). The error boxes represent the systematic uncertainties of the asymmetries. The size of the uncertainty boxes does not reflect the bin boundaries and is chosen for visualization purposes. The three panels display (a) inclusive neutron asymmetries, (b) BBC-tagged neutron asymmetries, and (c) BBC-vetoed neutron asymmetries.

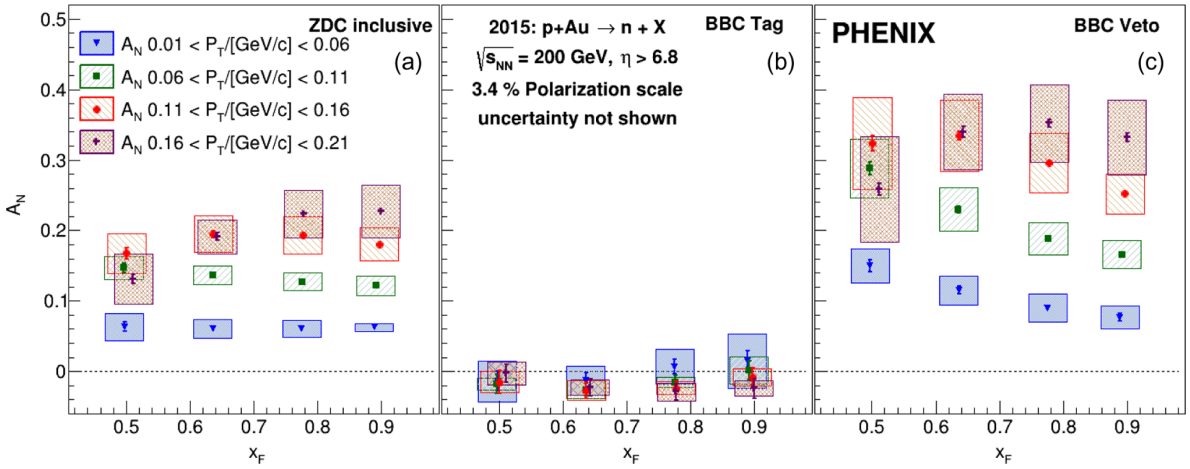

FIG. 8. Single spin asymmetries A_N for very forward neutrons in $p+\mathrm{Au}$ collisions as a function of x_F, in bins of transverse momentum p_T ([blue] triangles, [green] squares, [red] circles, and [purple] crosses in ascending order). The error boxes represent the systematic uncertainties of the asymmetries. The size of the uncertainty boxes does not reflect the bin boundaries and is chosen for visualization purposes. The three panels display (a) inclusive neutron asymmetries, (b) BBC-tagged neutron asymmetries, and (c) BBC-vetoed neutron asymmetries.

BBC-vetoed events a clear trend can be seen for lower transverse momenta where the asymmetries decrease with increasing x_F. At higher transverse momenta the uncertainties become too large to tell whether this trend continues. As mentioned previously, because the UPC based asymmetries closely rely on the resonances that can be formed, this is where one can expect the largest variation of the asymmetries with either kinematic variable.

VI. SUMMARY

In summary, the PHENIX experiment has measured single transverse spin asymmetries of very forward neutrons as a function of transverse momentum and longitudinal momentum fraction x_F. The asymmetries were extracted in $p+p$, $p+\mathrm{Al}$, and $p+\mathrm{Au}$ collisions and for neutrons that were either inclusively extracted or in (anti)correlation with hard collision-sensitive detectors. The asymmetries show a strong dependence on the collision system which can qualitatively be described by the interplay of hard interactions and ultraperipheral collisions which strongly depend on the charge of the colliding nucleus. These indications were corroborated by the (anti)correlated results that either enhance or reduce the contributions of the two competing processes. The asymmetries in hadronic processes appear to be negative and increase in magnitude with increasing transverse momentum to up to 10% while hardly any x_F dependence is visible. The UPC related asymmetries in contrast are positive and reach more than 30% in magnitude. Those are also initially rising with transverse momentum while for low x_F a subsequent decrease of the asymmetries is seen. Also at lower transverse momenta some differences in x_F are visible that in the model calculations originate from the different nucleon resonances contributing. The precision and the multi-dimensional dependence of these measurements will greatly improve the general understanding of how hadronic and photon-induced processes create single spin asymmetries at very forward rapidities and at small observed transverse-momentum scales.

ACKNOWLEDGMENTS

We thank the staff of the Collider-Accelerator and Physics Departments at Brookhaven National Laboratory and the staff of the other PHENIX participating institutions for their vital contributions. We acknowledge support from the Office of Nuclear Physics in the Office of Science of the Department of Energy, the National Science Foundation, Abilene Christian University Research Council, Research Foundation of SUNY, and Dean of the College of Arts and Sciences, Vanderbilt University (U.S.A), Ministry of Education, Culture, Sports, Science, and Technology and the Japan Society for the Promotion of Science (Japan), Natural Science Foundation of China (People's Republic of China), Croatian Science Foundation and Ministry of Science and Education (Croatia), Ministry of Education, Youth and Sports (Czech Republic), Centre National de la Recherche Scientifique, Commissariat à l'Énergie Atomique, and Institut National de Physique Nucléaire et de Physique des Particules (France), J. Bolyai Research Scholarship, EFOP, the New National Excellence Program (ÚNKP), NKFIH, and OTKA (Hungary), Department of Atomic Energy and Department of Science and Technology (India), Israel Science Foundation (Israel), Basic Science Research and SRC (CENuM) Programs through NRF funded by the Ministry of Education and the Ministry of Science and ICT

(Korea). Ministry of Education and Science, Russian Academy of Sciences, Federal Agency of Atomic Energy (Russia), VR and Wallenberg Foundation (Sweden), the U.S. Civilian Research and Development Foundation for the Independent States of the Former Soviet Union, the Hungarian American Enterprise Scholarship Fund, the US-Hungarian Fulbright Foundation, and the US-Israel Binational Science Foundation.

[1] W. Flauger and F. Monnig, Measurement of inclusive zero-angle neutron spectra at the ISR, Nucl. Phys. **B109**, 347 (1976).
[2] B. Z. Kopeliovich, I. K. Potashnikova, I. Schmidt, and J. Soffer, Damping of forward neutrons in pp collisions, Phys. Rev. D **78**, 014031 (2008).
[3] Y. Fukao *et al.*, Single transverse-spin asymmetry in very forward and very backward neutral particle production for polarized proton collisions at $\sqrt{s} = 200$ GeV, Phys. Lett. B **650**, 325 (2007).
[4] M. Togawa, Measurements of the leading neutron production in polarized pp collision at $\sqrt{s} = 200$ GeV, Ph.D. thesis, Kyoto University, 2008.
[5] A. Adare *et al.* (PHENIX Collaboration), Measurement of transverse-single-spin asymmetries for midrapidity and forward-rapidity production of hadrons in polarized $p + p$ collisions at $\sqrt{s} = 200$ and 62.4 GeV, Phys. Rev. D **90**, 012006 (2014).
[6] B. Z. Kopeliovich, I. K. Potashnikova, I. Schmidt, and J. Soffer, Single transverse spin asymmetry of forward neutrons, Phys. Rev. D **84**, 114012 (2011).
[7] C. Aidala *et al.* (PHENIX Collaboration), Nuclear Dependence of the Transverse-Single-Spin Asymmetry for Forward Neutron Production in Polarized $p + A$ Collisions at $\sqrt{s_{NN}} = 200$ GeV, Phys. Rev. Lett. **120**, 022001 (2018).
[8] G. Mitsuka, Recently measured large A_N for forward neutrons in $p \uparrow A$ collisions at $\sqrt{s_{NN}} = 200$ GeV explained through simulations of ultraperipheral collisions and hadronic interactions, Phys. Rev. C **95**, 044908 (2017).
[9] U. A. Acharya *et al.* (PHENIX Collaboration), Transverse momentum dependent forward neutron single spin asymmetries in transversely polarized $p + p$ collisions at $\sqrt{s} = 200$ GeV, Phys. Rev. D **103**, 032007 (2021).
[10] K. Adcox *et al.* (PHENIX Collaboration), PHENIX detector overview, Nucl. Instrum. Methods Phys. Res., Sect. A **499**, 469 (2003).
[11] R. Brun, F. Bruyant, F. Carminati, S. Giani, M. Maire, A. McPherson, G. Patrick, and L. Urban, *GEANT Detector Description and Simulation Tool* (1994), https://cds.cern.ch/record/1082634?ln=en.
[12] S. Roesler, R. Engel, and J. Ranft, The Monte Carlo event generator DPMJET-III, in *International Conference on Advanced Monte Carlo for Radiation Physics, Particle Transport Simulation and Applications (MC 2000)* (2000), p. 1033 [arXiv:hep-ph/0012252].
[13] T. Sjöstrand, L. Lönnblad, and S. Mrenna, PYTHIA 6.2: Physics and manual, arXiv:hep-ph/0108264.
[14] T. Sjöstrand, S. Ask, J. R. Christiansen, R. Corke, N. Desai, P. Ilten, S. Mrenna, S. Prestel, C. O. Rasmussen, and P. Z. Skands, An introduction to PYTHIA 8.2, Comput. Phys. Commun. **191**, 159 (2015).
[15] S. R. Klein, J. Nystrand, J. Seger, Y. Gorbunov, and J. Butterworth, STARlight: A Monte Carlo simulation program for ultra-peripheral collisions of relativistic ions, Comput. Phys. Commun. **212**, 258 (2017).
[16] G. D'Agostini, A multidimensional unfolding method based on Bayes' theorem, Nucl. Instrum. Methods Phys. Res., Sect. A **362**, 487 (1995).
[17] T. Adye, Unfolding algorithms and tests using RooUnfold, in *PHYSTAT 2011* (CERN, Geneva, 2011), p. 313.
[18] R. Brun and F. Rademakers, ROOT: An object oriented data analysis framework, Nucl. Instrum. Methods Phys. Res., Sect. A **389**, 81 (1997).
[19] A. Höcker and V. Kartvelishvili, SVD approach to data unfolding, Nucl. Instrum. Methods Phys. Res., Sect. A **372**, 469 (1996).
[20] The RHIC Polarimetry Group, Note No. 490, (2018).
[21] Gaku Mitsuka (private communication), based on [8].
[22] V. Guzey and M. Strikman, Proton-nucleus scattering and cross section fluctuations at RHIC and LHC, Phys. Lett. B **633**, 245 (2006).
[23] G. Mitsuka, Forward hadron production in ultra-peripheral proton–heavy-ion collisions at the LHC and RHIC, Eur. Phys. J. C **75**, 614 (2015).
[24] D. Drechsel, S. S. Kamalov, and L. Tiator, Unitary isobar model- MAID2007, Eur. Phys. J. A **34**, 69 (2007).